Characterizing a New Fluorescent Protein for a Low Limit of Detection Sensing in the Cell-Free System

Caroline E. Copeland,[§] Jeehye Kim,[§] Pearce L. Copeland, Chloe J. Heitmeier, and Yong-Chan Kwon*

Read Online

| ACCESS | | Metrics & More | | Article Recommendations | | Supporting Information |

ABSTRACT: Cell-free protein synthesis-based biosensors have been developed as highly accurate, low-cost biosensors. However, since most biomarkers exist at low concentrations in various types of biopsies, the biosensor's dynamic range must be increased in the system to achieve low limits of detection necessary while deciphering from higher background signals. Many attempts to increase the dynamic range have relied on amplifying the input signal from the analyte, which can lead to complications of false positives. In this study, we aimed to increase the protein synthesis capability of the cell-free protein synthesis system and the output signal of the reporter protein to achieve a lower limit of detection. We utilized a new fluorescent protein, mNeonGreen, which produces a higher output than those commonly used in cell-free biosensors. Optimizations of DNA sequence and the subsequent cell-free protein synthesis reaction conditions allowed characterizing protein expression variability by given DNA template types, reaction environment, and storage additives that cause the greatest time constraint on designing the cell-free biosensor. Finally, we characterized the fluorescence kinetics of mNeonGreen compared to the commonly used reporter protein, superfolder green fluorescent protein. We expect that this finely tuned cell-free protein synthesis platform with the new reporter protein can be used with sophisticated synthetic gene circuitry networks to increase the dynamic range of a cell-free biosensor to reach lower detection limits and reduce the false-positive proportion.

KEYWORDS: cell-free protein synthesis, mNeonGreen, biosensor, low limit of detection, fluorescent protein, gene circuit
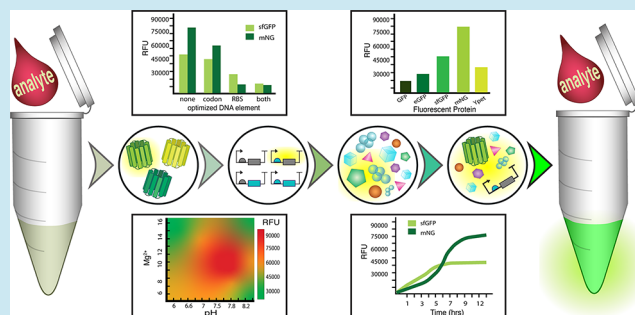
INTRODUCTION

The cell-free protein synthesis (CFPS) system has been proven as a powerful platform for advancing our ability to study, exploit, and expand the potential of applied biotechnology and synthetic biology.[1,2] With the system's unprecedented level of freedom and modularity to modify and control biological systems, the CFPS system allows for the prototyping of complex cellular functions by breadboarding genetic parts,[3−9] genetic circuits,[10−18] protein modifications,[19−22] and biosynthetic pathways.[23−26] These advantages unlock the opportunity to transform the system into a versatile in vitro biosensing platform. Sensing biological artifacts such as nucleic acids,[27−29] hormones,[30] vitamin levels,[31] harmful chemicals and compound levels,[32−35] heavy metals,[35,36] protein biomarkers,[37,38] and protein−protein interactions[39] can be done precisely, quickly, and inexpensively when utilizing the cell-free system (CFS).

These cell-free biosensors share the same core component of RNA and protein synthesis (transcription and translation) but differ in the way they detect the analyte and the cascade of events that occur between the detection, and RNA and protein synthesis. Cascade triggering methods and their targets include transcription factors (TFs) to detect harmful small molecules,

hormone receptors to detect endocrine disruptors, antibody−DNA conjugations to detect biomarker proteins, CRISPR-Cas proteins to differentiate between species variants, and riboregulators like the toehold switch to detect RNA associated with illnesses or riboregulators to detect fluoride.[40] Researchers often use combinatorial methods in the cascade, with the entire sequence of events being classified as a gene circuit.

A low limit of detection (LOD) is a crucial feature for developing CFS biosensors because biomarkers and other molecules of interest are often present at very low levels in various types of specimens.[41] Due to the frequent false-positive signals of low-cost, on-demand biosensors, researchers are required to add costly, time-consuming sample preparation processes. Another problem biosensors can come across is maximizing the dynamic range, which is the ratio between the leaky expression and the maximum expression (signal-to-noise
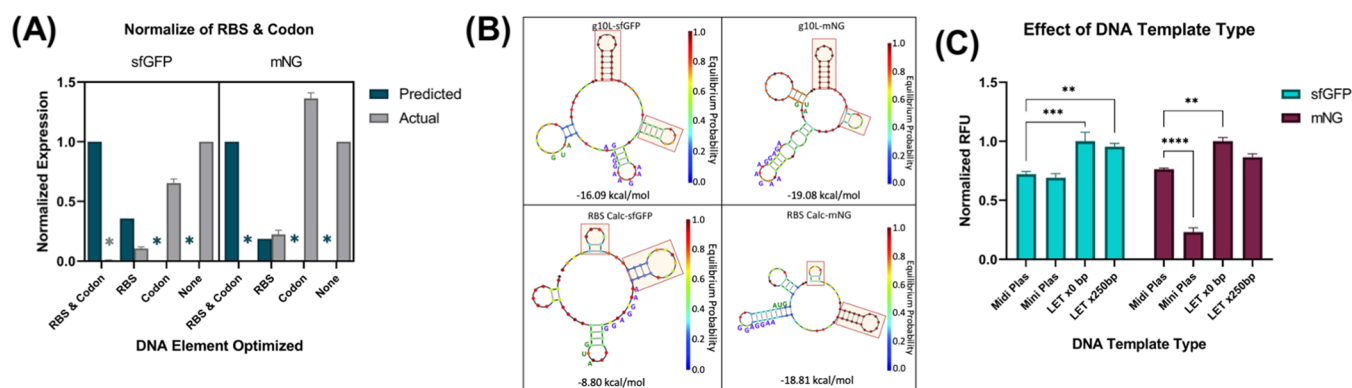
Figure 1. Effect of DNA elements and DNA template types on the fluorescent protein output. (A) RBS calculator predicted TIR compared to the actual fluorescent output (RFU) for the two fluorescent proteins. Colored "*" represent values too low to be seen on the graph. Predicted values were normalized to the highest value in each group. Actual values were normalized to the WT RFU expression in each group. All actual values for sfGFP and mNG were significantly different across DNA element optimization and compared against predicted values ($P < 0.0001$, $P < 0.05$ for mNG RBS predicted vs actual, two-way analysis of variance (ANOVA), Tukey). (B) NUPACK RNA prediction drawings of the sequences upstream of the RBS first 20 nucleotides for the *g10*-L sequence used in our WT expression and the RBS calculator enhanced TIR sequence. The standby site is highlighted in red, and the RBS site and start codon are spelled out in blue and green, respectively. At the bottom of each structure, it says "free energy of secondary structure", and the values are −16.09, −19.08, −8.80, and −18.08 kcal/mol, respectively. On the sides of the structure, it says "equilibrium probability". (C) sfGFP and mNG were expressed in four different template types. RFU values normalized to the highest expressed within protein group fluorescence output for miniprep plasmid showed the most variation between sfGFP and mNG, with mNG miniprep plasmid showing consistently significantly lower expression, while sfGFP did not show significantly lower expression (****$P < 0.0001$, two-way ANOVA, Tukey). LETx0bp showed slightly higher expression than the heavily purified Midiprep plasmid template (sfGFP ***$P < 0.001$, mNG using two-way ANOVA, Tukey). LETx250bp showed higher expression than Midiprep plasmids only for sfGFP expression (**$P < 0.01$ two-way ANOVA, Tukey). All experiments in (A) and (C) were run to completion (20 h) in the same conditions; data represented as mean ± standard deviation (SD), $n = 3$.

ratio). Having a larger dynamic range will help the biosensor reach a low LOD and allow the sensor to pick up on a larger range of low levels of analyte. For transcription factor (TF)-based cell-free biosensors, decreasing the amount of TF or increasing the amount of reporter DNA with the operator can aid in reaching a low LOD, but then the dynamic range could be lost.[34,35] Others that have had problems with dynamic range have had to lower their reporter DNA concentration, which lowers the LOD.[37] To increase the dynamic range, methods have been created to scale up the cascade input from the target molecule to a higher detectable level, known as genetic amplifiers or positive feedback loops. Examples of amplifiers include the activation of robust ligand-free TFs,[42,43] a TF-free bacteriophage RNA polymerase or sigma factor-endogenous RNA polymerase pair,[44] an antirepressor RNA aptamer,[35] or by a tag-specific protease targeting a repressor.[45] The issue with adding an amplifier feedback loop or an amplification step of the analyte is that if either one is triggered falsely, the signal will be much higher than what it would have been without that extra step.

One type of amplifier with the potential for a false-positive signal includes nucleic acid-based amplifiers, especially those that are isothermal reactions. These are very common for nucleic acid sensors because the DNA/RNA of interest can trigger a polymerase chain reaction (PCR)-like reaction. One popular example of a sensor that uses an amplifier includes the toehold switch that detects Zika virus from serum and uses nucleic acid sequence-based amplification (NASBA) as an amplification step to reach a low enough LOD to detect the virus concentration in human serum at 7.2×10^5 copies/mL (1.2 fM).[27] However, NASBA can create off-target amplification from a human serum sample full of other RNA molecules because of the difficulty of efficient primer binding to RNA.[46]

Here, we aim to amplify the output signal in other ways that do not involve the analyte but rather by increasing the signal of the output protein and maximizing the performance of the cell-free protein synthesis reaction overall. To achieve the overarching goal of this study, we investigated various cell-free conditions and components that can potentially improve cell-free biosensor development. One of the largest contributions to cell-free biosensors in this research involves introducing the robust fluorescent protein, mNeonGreen (mNG), which has been highlighted as the brightest fluorescent protein.[47,48] We achieved a 2.6 times higher signal from mNG than the commonly used superfold green fluorescent protein (sfGFP) in the CFS. We also compared the maturation time and fluorescence output rate to evaluate if mNG is comparable to the sfGFP.[49]

The other aim of this paper is to highlight various components a cell-free biosensor researcher might want to optimize to increase the reporter protein expression, our findings when optimizing these components to give them a starting point, and protein expression with different contaminants that typical cell-free biosensor target analytes reside. We investigated the DNA templates by optimizing different sequence elements and characterizing protein expression by template types. We assessed the ribosome binding site (RBS), 5′-untranslational region (UTR), spacer sequence, and codon usage to measure the DNA template-dependent cell-free protein synthesis capacity. In addition, we evaluated the cell-free protein synthetic tolerance on various additives and environmental matrix effects. We anticipate that the finely tuned CFS platform in this study can be used with sophisticated synthetic gene circuitry networks to increase the dynamic range of a cell-free biosensor to reach lower LOD and reduce the number of false-positive rates during the diagnosis.

■ RESULTS AND DISCUSSION

DNA Elements and Type Effect on Protein Expression. Optimizing and selecting DNA elements and expression templates significantly influence the protein expression level. Since one of this study's aims is to increase the output of the fluorescent protein to increase sensitivity capabilities and retain accuracy, we looked at optimizing these DNA characteristics. Potential cell-free biosensor researchers might not be aware that these characteristics can have large effects on protein expression or they may not know that some optimization tools that work well for whole-cell protein expression do not translate well to cell-free expression. Here, we aim to give those researchers a starting point for their reporter protein optimizations.

The ribosomal footprint and ribosome binding site (RBS) sequence have previously been shown to significantly impact protein synthesis, more than the promoter sequence, but in a more unpredictable way.[50,51] Even though the strength of the RBS relies heavily on the gene that is being translated due to mRNA structuring, a substantial amount of the currently provided part characterizations are unapplicable for the substitution of genes.[51] Therefore, the computational modeling of DNA structure combined with experimental screening has been performed to find patterns in the DNA elements and expedite the design−build−test (DBT) cycle for fast confirmation of the gene expression in the CFS. One of the popular computation tools is known as the RBS calculator.[51,52]

To see how well the computer-generated elements would predict protein synthesis, we only tested the highest in silico performing design of the 5′-UTR, RBS, and spacer region (ribosome footprint) and one output of the codon optimization for each of the fluorescent proteins. The RBS calculator has previously proven to be especially popular among in vivo protein expression studies;[53] however, here, we found the calculator does not fit to in vitro expression, even though the predicted translation initiation rate (TIR) from the RBS calculator is significantly higher than the wild type (WT) (Figure 1A). We found that the predicted translation initiation rate (TIR) values were opposite from the actual expression for both sfGFP and mNG, testing the optimization of the RBS, codon sequence, and both combined. This is almost expected since inserting new elements into DNA expressed in vivo is nonconventional but rather requires many variations until the desired function is reached.[54] This discordance is elevated when the system is taken in vitro where the expression environment becomes even more non-native. Another lab also discovered that the ribosome binding calculator was not suitable for their in vitro protein expression, showing the least out of the five they tested, but it had one of the highest RNA expression rates.[50] They were more successful with screening a subset of randomly generated RBS structures lacking strong structural elements.

The protein expression with our original RBS is significantly higher than the predicted RBS because we use the T7 phage gene 10 leader RNA (*g10*-L), which is a ribosome footprint that dramatically increases the protein expression of foreign genes in *Escherichia coli*. This gene 10 in the T7 phage codes for coat protein, which is made the most after infection, so it has to have an optimal 5′-UTR for the T7 RNA polymerase and *E. coli* ribosomes to overproduce foreign proteins.[55] Therefore, our 5′-UTR might already be at its optimal sequence for transcription and translation.

The mRNA is a single-stranded molecule that can form secondary structures by binding to itself, sometimes causing the RBS not to be available for the 30S ribosomal subunit to bind immediately. Thus, the 30S subunit must wait at a nonsequence-specific region flanked by a stable hairpin and the hairpin containing the RBS until the hairpin with the RBS opens so it can slide into place using linear diffusion and bind. This waiting region is known as the standby site, the most geometrically accessible, and requires the least amount of RNA unfolding.[56] NUPACK is a computer software that can predict these mRNA secondary structures (detailed methods in the Supporting Information). We analyzed the RNA structure of the 5′-UTR and the first 20 bp of the coding region for our wild-type genes and RBS optimized genes. The *g10*-L sequence has very prominent hairpins upstream of possible standby sites (highlighted in red) and then a low structure around the RBS site and start codon (spelled out in blue and green, respectively) (Figure 1B, top). The calculated RBS footprints with the first 100 bp show a less prominent standby site and more structures around the RBS site (Figure 1B, bottom). The TIR is directly correlated to the amount of energy the ribosome must spend on its own, doing things such as weaving through tall hairpins, unfolding RNA, and ribosomal distortion—with the more expended, the less left for translation initiation.[57] Possibly, the structures of the *g10*-L are more favorable for conserving the ribosome's initial energy than the calculated ones, especially in a more dilute environment (the CFS) compared to the whole cell, which could change the electrostatic interactions of the ribosome and RNA even more.

Not only does the RBS sequence make a difference in how well RNA is transcribed but so does the codon sequence. Researchers have found that the high GC content in the coding region creates more protein, and the cell's codon usage can impact protein expression levels greatly by influencing the folding speed and efficiency of the protein during translation.[50,58,59] This is mainly due to the charged tRNA pools, the cell's usage of synonymous codons, and rare codons in recombinant genes, which makes protein synthesis stall or perform incorrectly if the rare tRNA's become depleted.[60,61] The benefits of codon optimization for recombinant protein synthesis in the CFS have been shown before, resulting in a 7.4-fold increase in protein for the cell extract void of rare tRNA expression.[62] We found that codon optimizing increased the mNG expression (1.3 times) but decreased the sfGFP expression (0.8 times) (Figure 1A). Since mNG was not codon-optimized for *E. coli* codon usage and sfGFP was already established as a model reporter protein in *E. coli*, so sfGFP's codon usage is possibly already well coordinated to fit for *E. coli*.

The type of DNA template used in the CFS plays a crucial role in the speed of design−build−test (DBT) cycles. Previously, it has been demonstrated that linear DNA expression templates (LETs) amplified by PCR perform very well in the CFS when extra base pairs (bp) are added to protect the important DNA elements (5′- and 3′-UTRs) from any degradation at the ends, some showing 26-fold (mRFP1) and 12-fold (GFPmut3b) increase in expression[50] and 6-fold increase (deGFP)[63] from LETs with no buffer of base pairs. In our experiments, we did not see a significant increase in expression by adding 250 extra base pairs to the 5′ and 3′ ends of the LET (upstream of the promoter and downstream of the terminator), but we observed a small increase in expression
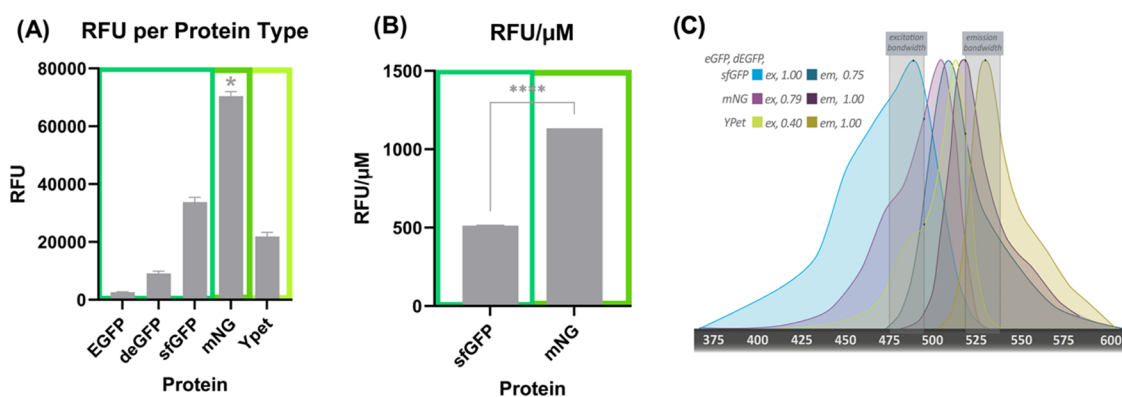
Figure 2. Comparing common CF fluorescent proteins. (A) eGFP, deGFP, sfGFP, mNG, and YPet were synthesized in the CFS in LET DNA format and compared using the same filters. mNG was significantly brighter than all other fluorescent proteins tested (*$P < 0.0001$ using one-way ANOVA); data represented as mean ± SD, $n = 3$. (B) RFU/μM comparison of sfGFP and mNG showing that mNG is significantly brighter than sfGFP and not just making more protein, with an RFU/μM ratio 2.1-fold higher than sfGFP (****$P < 0.0001$ using an unpaired t-test); data represented as mean ± SD, $n = 3$. (C) Comparing the fluorescent excitation−emission spectra of all five proteins. eGFP, deGFP, and sfGFP had extremely similar peaks, so they were included as one (blue), mNG in purple, and YPet in yellow. The maximum relative intensities for excitation and emission of the proteins, given our filters, were mentioned in the top left corner for each protein and marked on the graph in black. The light white panels signify our filters' bandwidths.

compared to the plasmid templates of the fluorescent proteins (Figure 1C). Even though the expression of LETs with the 250 bp buffer was slightly lower than those without, we decided to use the 250 bp buffer LETs from there on out to remove some possibility of gene degradation during storage. The exonuclease inhibitor GamS can also increase the expression from linear DNA templates with 250 bp buffer by 26% for deGFP since it helps protect the ends from degradation.[63] When a final concentration of 2 μM of GamS was used in our experiments with linear DNA with 250 bp buffer on the 5′ and 3′ ends, we saw a 14.0 ± 2.5% increase in fluorescence for sfGFP and 24 ± 5.1% increase for mNG (Figure S1). We also tested Miniprep-level purified plasmid DNA templates since they are much faster and less expensive to purify than plasmids purified at the midi and maxiprep levels. Interestingly, the sfGFP expression was not affected by the lack of extra purification steps, but mNG was significantly affected, with an ∼70% decrease, even after repeating the experiment multiple times (Figure 1C). Additional isopropanol precipitation in the last step of midi and maxiprep purification may affect the plasmid structure transition between supercoil and circular in different DNA sequences and eventually affect the overall protein production level difference between sfGFP and mNG.[64]

The maximum concentration of plasmid DNA for the maximum amount of protein has been shown to plateau at 5−15 nM of DNA concentration when using endogenous RNA polymerase for transcription. In another study, however, the DNA concentration of plasmid and LET was not reflected in the overall transcription and translation efficiency using T7 RNA polymerase.[4,63] We also observed the same phenomenon when we compared plasmid DNA and LETs of sfGFP (Figure S2). We found that the plasmid concentration plateau was lower than previous reports using endogenous RNA polymerase, with their plateaus occurring around 5−10 nM and decreasing soon after, but we displayed a significantly higher protein production from the initial concentration. However, gene expression with LET did not have a clear plateau, and the expression was extremely variable across concentrations.

mNeonGreen, a Brighter Fluorescent Protein Than Those Commonly Used. Using the brightest fluorescent protein available as the reporter protein for the biosensor is

also an important factor in decreasing the limit of detection. In this paper, we discuss the usage and production of mNG in the CFS for the first time, as an extremely bright reporter protein that can be used with CF sensors. mNG is not derived from the original green fluorescent protein variants from *Aequorea victoria* but is derived from the cephalochordate *Branchiostoma lanceolatum* and is the monomeric variant of the tetramer LanYFP.[47] It is the brightest monomeric green or yellow fluorescent protein reported to date. It has a high quantum yield (∼0.80) and extinction coefficient (∼116,000 M^{-1} cm^{-1}). It has shown a high acid tolerance, with a pK_a of 5.7, making it a good candidate for long-term expression in the CFS, which turns acidic as ATP is consumed.[65]

In CF reactions, green fluorescent proteins provide the fastest response and lowest LOD compared to red fluorescent reporters and colorimetric LacZ output,[66] so we compared the new mNG protein with the popular green proteins: sfGFP, deGFP, eGFP, and YPet in the CFS. The fluorescence characterizations of each protein can be found in Table S2. deGFP[4] was created to be more translatable in the CFS than eGFP, but here we show that mNG is 7.75-fold brighter than deGFP and 26.81-fold brighter than eGFP and even significantly brighter than the superfolder GFP, 2.08-fold, a commonly used protein for CF sensors due to its brightness (Figure 2A). mNG is not just brighter than the commonly used sfGFP because the system is making more of the protein. As shown in Figure 2B, the RFU/μM ratio of mNG is 2.1-fold higher than sfGFP, meaning the protein itself is brighter than sfGFP in our CFS. mNG was also compared to Ypet, a yellow fluorescent protein, and it showed to be brighter by 3.21-fold. The excitation and emission spectra for all of the fluorescent proteins are shown in Figure 2C, with sfGFP, deGFP, and eGFP sharing the same curves.

Fluorescent Output Variability with Environmental Changes. Matrix effects[31−33] caused by non-native reagents and possible harmful molecules in the CFS sensor platform can unexpectedly interfere with the sensor's function. These substances can range anywhere from buffers to samples stored in biological components. To characterize the CFS's tolerance to these foreign substances, we analyzed protein expression in
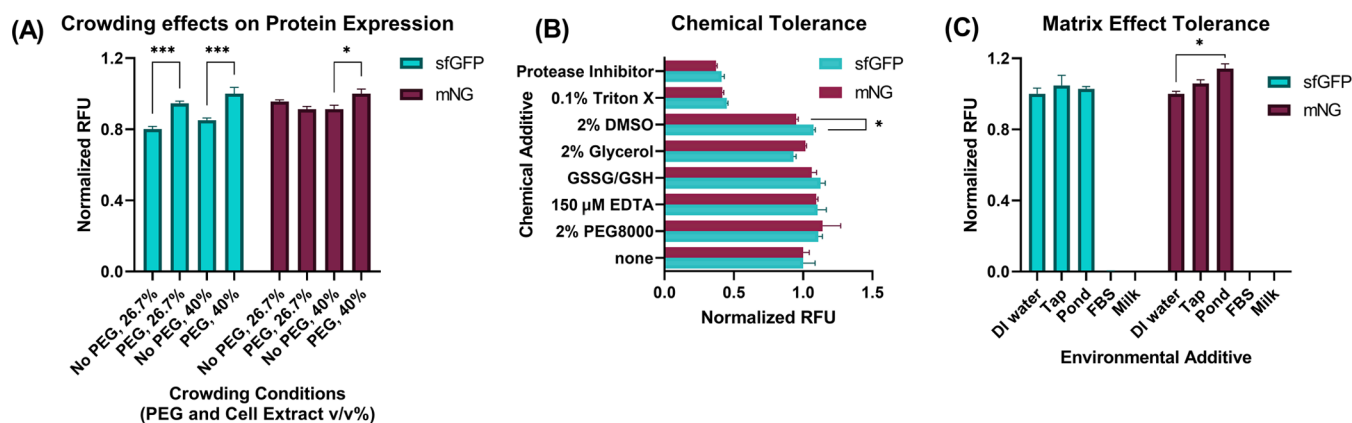
Figure 3. Fluorescent output and variability with environmental changes. (A) Crowding effects on the protein expression for sfGFP and mNG. Crowding was simulated by increasing the extract concentration and by adding 2% PEG 8000. Expression was significantly increased for sfGFP in both extract concentrations and mNG for the higher extract concentration (*$P < 0.05$, ***$P < 0.001$, two-way ANOVA, Tukey). RFU values were normalized to the highest in each protein group separately. (B) sfGFP and mNG tolerance to different chemical additives. sfGFP and mNG tolerated the chemical additives similarly, but sfGFP tolerated 2% dimethyl sulfoxide (DMSO) more than mNG (*$P < 0.05$, two-way ANOVA, Tukey). RFU values are normalized to the highest in each protein group separately. (C) Comparing the ability of sfGFP and mNG to tolerate matrix effects with additions of 26.7% (v/v). Both could tolerate tap water and pond water well, with mNG even expressing significantly higher in pond water than in DI water (*$P < 0.05$, two-way ANOVA, Tukey). Protein synthesis did not occur with additions of fetal bovine serum (FBS) and whole milk. All data (A−C) represented as mean ± SD, $n = 3$.
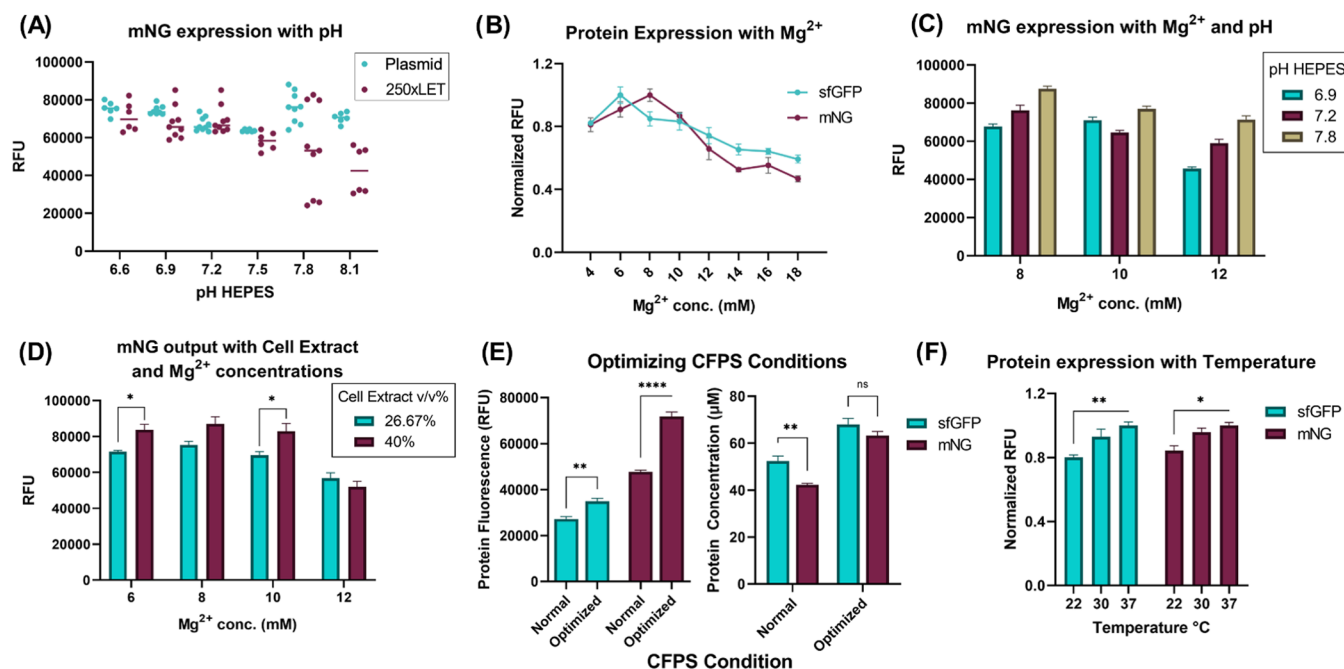
Figure 4. Characterizing protein expression and optimizing conditions. (A) mNG expression with different pH values of the buffer varies depending on the DNA template type. LET show more variability than plasmid DNA gene expression. HEPES buffer of pH 7.8 shows the highest expression. Data represented as mean ± SD, $n = 6$–9. (B) mNG and sfGFP expression with varying Mg^{2+} concentrations. Both show similar patterns but with sfGFP producing its most at 6 mM and mNG at 8 mM. Data represented as mean ± SD, $n = 3$. (C) mNG expression with different Mg^{2+} concentrations and HEPES pH in the CFPS reaction. The pattern of low to high expression with the increase in pH was similar across Mg^{2+} concentrations, as well as a high expression with decreasing Mg^{2+}, except for 10 mM pH 6.9. Data represented as mean ± SD, $n = 3$. (D) mNG expression with varying Mg^{2+} concentrations and cell extract v/v%. Adding more cell extract increases the expression significantly in Mg^{2+} concentrations of 6 and 10 mM (*$P < 0.05$, two-way ANOVA, Tukey). Data represented as mean ± SD, $n = 3$. (E) mNG and sfGFP expression in optimized conditions compared to normal. The RFU value is shown on the right and protein concentration (μM) on the left. mNG has a higher RFU/μM ratio (Figure 2B); therefore, the μM was slightly lower than sfGFP in optimized conditions, while significantly lower in the normal conditions (**$P < 0.01$, ****$P < 0.0001$, two-way ANOVA, Tukey). Data represented as mean ± SD, $n = 4$. Fluorescence captured at a lower gain (48) here. (F) mNG and sfGFP expression with different temperatures. sfGFP expression is more significantly lowered at room temperature from 37 °C than mNG (*$P < 0.05$, **$P < 0.01$, two-way ANOVA, Tukey). RFU values were normalized to the highest in each protein group separately. Data represented as mean ± SD, $n = 3$.

common additives, storage buffers, and environmental contaminants.

To test whether crowding due to extra molecules in a biopsy or storage additive negatively affects protein expression, we

measured the fluorescent output of sfGFP and mNG with 2% poly(ethylene glycol) (PEG) 8000 and increased the cell extract concentration in the reaction mixture (26.7−40.0% v/v). Interestingly, sfGFP showed more evident signal flux at both crowding conditions with increased expression, whereas mNG maintained consistent signal outputs (Figure 3A). Although both the sfGFP and mNG are fluorescent proteins, increased cell extract concentration and additional crowding agent can affect their signal flux due to different protein maturation and fluorescent outcome speeds (Figure 5).

Next, we conducted the chemical tolerance test for sfGFP and mNG to compare the previous report[63] and the matrix effect tolerance test. Both proteins tolerated the chemical additives and were not significantly different from each other (according to a two-way ANOVA), with the exceptions of 0.1% Triton X and protease inhibitor, which reduced both proteins' output signals by 55−60% (Figure 3B). Notably, Triton X and protease inhibitors are frequently used for the eukaryotic cell lysis process and can potentially interrupt the output signals when sensing specimens from the eukaryotic cells.

We then introduced common environmental additives, including tap water, pond water, whole milk, and fetal bovine serum, to the system that might contain an analyte of interest in the future. Previous research had shown that the CFS could perform in the presence of RNase A when RNase inhibitor was presented. Since the RNase inhibitor is costly, we chose to use polyvinylsulfonic acid (PVSA), which has been shown to mimic the functions of commercially available RNase inhibitors in the CFS with inhibiting RNases.[67] PVSA was added to all reactions containing an environmental additive. Unfortunately, we did not obtain the same results when we used cell-culture media designated fetal bovine serum (FBS), which is a sample abundant with RNases and closer to a real-world application sample. Another study has added human serum to the CFS that enabled the synthesis of proteins with murine RNase inhibitor and only added a 14% final volume fraction of serum to the reaction, while we added 26% with PVSA.[68] Interestingly, pond water and tap water performed very well in the CFS. However, FBS and milk additives suppressed the output signals completely (Figure 3C).

System Optimization for mNG. In the cell-free protein synthesis reaction, many components are added, some having a higher impact on the protein synthesis outcome than others and some needing personalization for the specific protein being made.[62,69] Here, we highlight and display those settings that have the largest impact on protein expression so that cell-free biosensor researchers can become aware of these tuning opportunities to increase their reporter protein expression. Also, since it had not been synthesized in this system before, we screened mNG expression with different CFPS conditions, including pH, Mg^{2+} concentration, cell extract concentration, reaction temperature, and combinations of these mentioned. We also highlight CFS settings.

To change the pH of the system, we used N-(2-hydroxyethyl)piperazine-N'-ethanesulfonic acid (HEPES) buffer with different pH values. HEPES is used to stabilize the system's pH, so changing this can have a big impact on the final pH of the system (Table S3).[69] We first used 250× bp LETs of mNG in these different pH environments but the trend was not consistent (Figure 4A). We then switched to using plasmids to express the proteins and noticed a more consistent trend, with the HEPES buffer (pH 7.8) showing the highest expression of mNG (Figure 4A). We concluded that the expression from LETs could vary much more across pH values than plasmids; therefore, we used plasmids for the remainder of the experiments. Data for sfGFP was not shown but had the same trend. mNG and sfGFP expression levels were characterized at different final Mg^{2+} concentrations (4−18 mM), showing a similar trend for both but with sfGFP producing its most at 6 mM and mNG at 8 mM, respectively (Figure 4B). Then, mNG expression was tested in the combination of Mg^{2+} concentrations (8−12 mM) and pH values (6.9−7.8). The pattern of low to high expression with the increase in pH was similar across Mg^{2+} concentrations, as well as a high expression with decreasing Mg^{2+}, except for 10 mM Mg^{2+} and pH 6.9 (Figure 4C).

Since buffer B (S30 buffer) of the cell extract contributes to the final concentration of Mg^{2+} in the cell-free reaction, we tested mNG expression in different concentrations of cell extracts across varying Mg^{2+} concentrations. The extra Mg^{2+} from buffer B did not influence the pattern of mNG synthesis across Mg^{2+} concentrations but adding more extract did improve the expression significantly in Mg^{2+} concentrations of 6 and 10 mM and slightly in 8 mM concentration (Figure 4D). This increase can be attributed to the extra TX-TL components in the extract. After the optimal conditions of pH, Mg^{2+}, and cell extract concentration were verified, we then combined them into one experiment and compared them with the previously optimized CFPS (normal) conditions of our lab. These optimal conditions included a HEPES buffer (pH 7.8), 40% v/v cell extract, 2% PEG 8000, and 6 mM (mNG) and 8 mM (sfGFP) Mg^{2+}. This is compared to the previously used conditions: HEPES buffer (pH 7.2), 26.7% v/v cell extract, no PEG 8000, and 12 mM Mg^{2+}. These optimal CFPS conditions were able to increase fluorescence outputs by 50.3 and 28.4% for mNG and sfGFP, respectively (Figure 4E, left). The amount of protein synthesized in the normal conditions was 42.32 ± 1.22 μM or 1.13 ± 0.03 mg/mL for mNG and 52.41 ± 4.3 μM or 1.41 ± 0.12 mg/mL for sfGFP. The amount of protein synthesized in the optimal conditions was 63.33 ± 3.39 μM or 1.69 ± 0.09 mg/mL for mNG and 68.05 ± 5.07 μM or 1.83 ± 0.14 mg/mL for sfGFP (Figure 4E, right). Notably, mNG showed a brighter signal output with a higher RFU/μM or mg/mL ratio. Therefore, its protein concentration will be lower than sfGFP even though the RFUs are high. Lastly, protein synthesis was tested at different temperatures (22 °C (room temperature), 30 °C, and 37 °C) to compare the fluorescent signal outputs at various sensing temperatures. Both proteins had a slight drop in protein expression at room temperature, but mNG was able to tolerate it slightly more than sfGFP, making it a good candidate for a point-of-care reporter protein (Figure 4F). Throughout the optimization process, from sfGFP expression at normal conditions to mNG at optimal conditions, fluorescence readout was able to be increased 2.64-fold, which is a significant increase to aid in detecting low levels of analyte in the CFS while still maintaining a distinguishable readout.

Maturation and Fluorescent Output Speed. Maturation and fluorescent output speed can be an important factor for biosensor construct advertising as rapid to consider. Here, we compared these speeds of sfGFP with the new mNG. The maturation process of the GFP family involves the folding of the β-barrel, torsional rearrangements, cyclization, and oxidation and dehydration of the chromophore.[70] The "superfolder" GFP compared in this study was engineered to
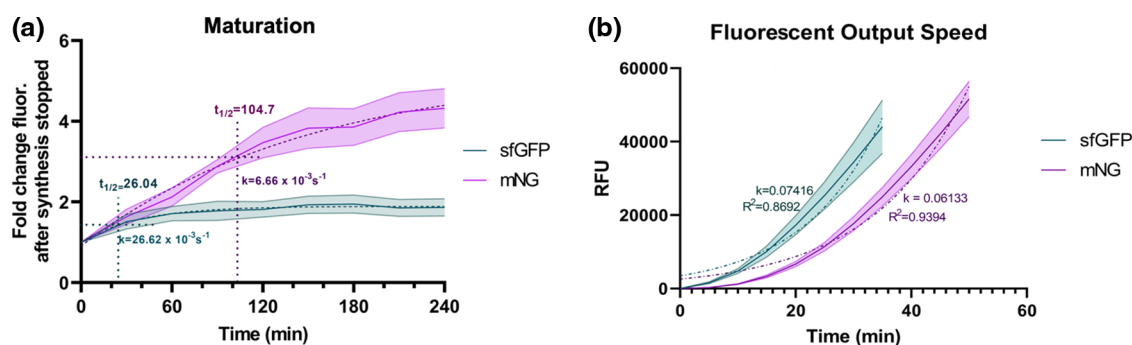
Figure 5. Fluorescence kinetics of sfGFP and mNG. (A) Maturation of sfGFP and mNG. Fluorescence fold change after synthesis had ceased. sfGFP maturation rate $k = 26.62 \times 10^{-3}$ s^{-1} and half-time of maturation ($t_{1/2}$) 26.04 min. mNG maturation rate $k = 6.66 \times 10^{-3}$ s^{-1} and half-time of maturation $t_{1/2} = 104.7$. (B) Fluorescent output speed of sfGFP and mNG. sfGFP exponential growth rate $k = 0.07416$ and mNG $k = 0.06133$. RFU was measured on a different machine than in the other experiments. Panels (A) and (B) are represented as mean $\pm$ SD, $n = 3$.

fold more robustly and faster with more stability than the regular reporter GFP. These enhancements contribute to a generation of higher fluorescence signal outputs.[49] We compared the protein maturation rate with the actual fluorescent signal outputs to apply mNG as an alternative fluorescent protein for the CF sensor. mNG has a comparable maturation to sfGFP in the CFS when measuring to a certain fold change, but mNG then keeps maturing to become even brighter (Figure 5A). sfGFP shows a 4-fold higher maturation rate $k = 26.62 \times 10^{-3}$ s^{-1}, and a 4-fold shorter half-time of maturation ($t_{1/2}$) is 26.04 min when compared to mNG rate $k = 6.66 \times 10^{-3}$ s^{-1} and half-time $t_{1/2} = 104.7$, but mNG shows a 2.32-fold greater fold change (4.322 ± 0.846) after the translation has ended than sfGFP (1.867 ± 0.370). This maturation experiment was conducted by allowing the reaction to run for 75 min and then immediately putting the tubes on an ice slush for 5 min. Then, the tubes were stored at 4 °C.

The rate of fluorescent output was tested in a quantitative PCR (qPCR) machine instead of the fluorescent plate reader since the former is more sensitive at reading smaller fluorescence output and can take multiple measures over time without evaporation. However, the fluorescence of sfGFP and mNG becomes too much for the qPCR machine to read, so we only measured the first few minutes to obtain the initial output rate. The rate of the fluorescent output showed that the fluorescent proteins fluoresced about 10 min apart from each other, with sfGFP in the lead (Figure 5B). Although mNG fluorescence fits more of an exponential pattern with a higher R^2 value (0.9394) than sfGFP ($R^2 = 0.8692$), they are both able to be visualized by the naked eye at around the 45 min mark when DNA template concentrations are close to saturation points in a 15 μL reaction. Overall, both proteins express fluorescence promptly in the CFS.

CONCLUSIONS

In this research, we have highlighted various components involved in building a robust cell-free biosensor that impacts protein synthesis to provide the researchers with optimal starting points for cell-free biosensor development. Having the knowledge of the optimized settings can greatly enhance the cell-free biosensor's dynamic range by starting with our given optimized data points instead of adding signal amplifiers between the data collection and output signal, thus possibly reducing the background and false-positive signal. This knowledge also allows the researcher to increase the output signal of the final reporter protein to see the reaction occurring

from the analyte at smaller concentrations, therefore lowering the limit of detection while retaining system accuracy. Sensitivity can also be increased in this way since the output signal becomes easier to measure for lower limits. However, it is more important for sensitivity to have the gene expression able to be triggered in the first place by these lower concentrations of the analyte.

We improved the fluorescence output of mNG in the CFS by 2.64-fold when compared to that of sfGFP and characterized protein synthesis in different conditions to offer mNG as an alternative fluorescent protein to achieve a low LOD. This was accomplished by first introducing a brighter fluorescent protein, mNeonGreen. Next, we identified more favorable DNA settings in the CFS with codon optimization, clarifying the optimal RBS, 5′-UTR, and spacer sequence and finding the optimal DNA template and type. We also characterized the fluorescent signal outputs of mNG and sfGFP while enduring different matrix effects from biological samples and possible CFS additives. Comparing mNG to the "superfolder" sfGFP, we found that mNG matured slower than sfGFP but reached the fluorescent maturation plateau point at the same time and surpassed it with a 2.32-fold greater change in maturation. Lastly, we optimized reaction conditions through a systemic optimization process of Mg^{2+} concentration, pH, percentage of cell extract, and molecular crowding conditions. In conclusion, these combinations can be used to increase the dynamic range of a CF sensor by optimizing the fluorescent signal output itself instead of amplifying the target analyte, so sensors can reach a lower LOD while keeping the number of false positives low.

METHODS

Materials. *E. coli* strains subcloning efficiency *DH5α* [genotype F$^-$ Φ80*lac*ZΔM15Δ(*lacZYA-arg*F) U169 *rec*A1 *end*A1 *hsd*R17(r$_K^-$, m$_K^+$) *phoA sup*E44 *thi*-1 *gyr*A96 *rel*A1 λ-] and BL21 star (DE3) [genotype F$^-$ *ompT hsdS*$_B$ (r$_B^-$ m$_B^-$) *gal dcm rne*131 (DE3)] were used for plasmid cloning and a source of the cell extract, respectively (Invitrogen, Waltham, MA). The *E. coli* cells were grown in either Luria−Bertani (LB) media (10 g/L of tryptone, 5 g/L of yeast extract, 10 g/L of sodium chloride in Milli-Q water) or 2× YTPG media (16 g/L of tryptone, 10 g/L of yeast extract, 5 g/L of sodium chloride, 7 g/L of potassium phosphate dibasic, 3 g/L of potassium phosphate monobasic, pH 7.2, and 0.1 M of glucose in Milli-Q water). CFS components including *E. coli* total tRNA mixture (from strain MRE600) ATP, GTP, CTP, UTP,

phosphoenolpyruvate (PEP), 20 amino acids, and other materials were purchased from Sigma-Aldrich (St. Louis, MO), Alfa Aesar (Haverhill, MA), and Fisher Scientific (Hampton, NH).

DNA Preparation. The optimal RBS for every gene was found using the De Novo DNA web tool known as the RBS calculator.[51] Primer extension was used to add different RBS footprint sequences to sfGFP and mNG. The codon-optimized versions of sfGFP and mNG sequences were prepared using the codon optimization tool for *E. coli* codon usage bias (strain K12) (Integrated DNA Technologies, Coralville, IA) and inserted into pJL1 plasmid using Gibson Assembly. Plasmids were transformed into DH5α electrocompetent cells for cloning and purification (E.Z.N.A. Plasmid DNA Midi Kit, Omega BioTek, Norcross, GA) for sequencing and cell-free reaction, respectively.

Linear templates were prepared by PCR and subsequent purification (E.Z.N.A. Cycle Pure Kit, Omega BioTek, Norcross, GA). The oligomer sequences are listed in Table S1. The amplified region included buffer sequences (250 bp each at 5′- and 3′-ends) upstream of the promoter and downstream of the terminator sequences unless otherwise noted (Table S1). The PCR products were verified on a 1% agarose to confirm the size and low off-target amplification. The DNA concentrations were measured with the BioTek Synergy HTX multimode reader using a Take3 Micro-Volume Plate.

Preparation of Cell Extract. Cell extract was prepared, as described previously.[71,72] Briefly, overnight cultured *E. coli* BL21 Star (DE3) in LB media was inoculated to sterilized 1 L 2× YTPG media in a 2.5 L baffled Tunair shake flask and the cells were cultured at 37 °C with vigorous shaking at 250 rpm. The optical density of the cells was monitored by the UV−vis spectrophotometer (Genesys 6, Thermo Fisher Scientific, Waltham, WA) (Figure S3) and induced to overexpress T7 RNA polymerase at OD$_{600}$ 0.6 with 1 mM of isopropyl β-D-1-thiogalactopyranoside (IPTG) (Figures S3 and S4). Cells were harvested at the mid-exponential phase (OD$_{600}$ 3.0) by centrifugation (5000 RCF at 4 °C for 15 min). Cell pellets were then washed with buffer A (dithiothreitol (DTT) added, pH 7.8) three times, flash-frozen in liquid nitrogen, and stored at a −80 °C freezer until use. Cell pellets were used within the same week to ensure maximum activity. Cell pellets were thawed on ice and then resuspended with buffer B (no DTT, pH 8.2) with 1 mL of buffer B for 1 g of wet cell mass and transferred into microtubes in 1 mL aliquots for lysis. The sonicator (Q125, Qsonica, Newtown, CT) with a 1/8 in. diameter probe was set to 20 kHz frequency, 50% amplitude, and 10 s on and 10 s off. To minimize protein degradation by heat, the tubes of cells were kept in ice water during sonication. The number of joules was determined by the equation found previously,[72] which equates to 537 J for 1 mL of resuspended cells. Three microliters of 1 M DTT was added per 1 mL lysate. The tubes were then centrifuged at 12,000 RCF at 4 °C for 10 min, and the supernatant was taken. Run-off and dialysis were not performed for the experiments in this study as we found them to be inhibitory, especially for LET DNA (Figure S5). The cell extract used in CFPS reactions was aliquoted and flash-frozen in liquid nitrogen and stored at a −80 °C freezer until use. The extract aliquots were only thawed for the reaction they were used for and not reused again to ensure the activity.

Cell-Free Protein Synthesis. Cell-free protein synthesis reactions were carried out in 1.5 mL microtubes in an incubator. The reaction volume was 15 μL with the following components: 1.2 mM ATP; 0.85 mM each of GTP, UTP, and CTP; 34.0 μg/mL of L-5-formyl-5,6,7,8-tetrahydrofolic acid (folinic acid); 170.0 μg/mL of *E. coli* tRNA mixture; 130 mM potassium glutamate; 10 mM ammonium glutamate; 12 mM magnesium glutamate; 2 mM each of 20 amino acids; 57 mM of HEPES buffer (pH 7.2, except for the pH experiments in Figure 4); 0.4 mM of nicotinamide adenine dinucleotide (NAD); 0.27 mM of coenzyme A; 4 mM of sodium oxalate; 1 mM of putrescine; 1.5 mM of spermidine; 33 mM phosphoenolpyruvate (PEP); and 27% v/v of cell extract. DNA was added at 13.3 μg/mL for plasmid DNA. Linear DNA final concentrations varied depending on length but were around 4.95 μg/mL for LETs without buffer sequences and 7.58 μg/mL for LETs with 250 bp buffer sequences. For the matrix effect experiments, samples were added at 26.67% of the final volume. Reactions were run for 20 h to ensure completion at 30 °C unless otherwise mentioned.

Quantitative Analysis of Fluorescent Proteins. The fluorescence intensity of the synthesized fluorescent proteins was measured by the multiwell plate fluorometer (Synergy HTX, BioTek, Winooski, VT). Five microliters of the cell-free synthesized fluorescent protein and 45 μL of Milli-Q water were mixed in a 96-well half-area black plate (Corning Incorporated, Corning, NY). The plate was mixed in the plated reader orbitally at a medium speed for 15 s and read at a height of 1.5 mm with a gain of 48. The excitation and emission spectra are 485 and 528 nm, respectively. The cell-free synthesized protein was visualized by Coomassie blue staining after protein gel electrophoresis using precasted 4−12% bis−tris gradient gel (Invitrogen, Waltham, MA) (Figure S6).

Statistical Analysis. Statistical analyses were conducted using Graphpad Prism 8.4.3 (GraphPad Software) with a 5% significance level. For the parametric analysis of data from quantification of the synthesized protein, a two-way ANOVA followed by Dunnett's test was used.

■ ASSOCIATED CONTENT

Ⓢ Supporting Information

The Supporting Information is available free of charge at https://pubs.acs.org/doi/10.1021/acssynbio.2c00180.

> Additional methods, supporting Figures S1−S6, supporting tables including DNA sequence information, characteristics of fluorescent proteins, and pH variations (PDF)

■ AUTHOR INFORMATION

Corresponding Author

Yong-Chan Kwon − *Department of Biological and Agricultural Engineering, Louisiana State University, Baton Rouge, Louisiana 70803, United States; Louisiana State University Agricultural Center, Baton Rouge, Louisiana 70803, United States;* ⓞ orcid.org/0000-0002-7551-6007; Email: yckwon@lsu.edu

Authors

Caroline E. Copeland − *Department of Biological and Agricultural Engineering, Louisiana State University, Baton Rouge, Louisiana 70803, United States*

Jeehye Kim − *Department of Biological and Agricultural Engineering, Louisiana State University, Baton Rouge, Louisiana 70803, United States*

Pearce L. Copeland − *Department of Biological and Agricultural Engineering, Louisiana State University, Baton Rouge, Louisiana 70803, United States*

Chloe J. Heitmeier − *Department of Biological and Agricultural Engineering, Louisiana State University, Baton Rouge, Louisiana 70803, United States*

Complete contact information is available at:
https://pubs.acs.org/10.1021/acssynbio.2c00180

Author Contributions

Notes

The authors declare no competing financial interest.

■ ACKNOWLEDGMENTS

■ REFERENCES

(1) Carlson, E. D.; Gan, R.; Hodgman, C. E.; Jewett, M. C. Cell-free protein synthesis: applications come of age. *Biotechnol. Adv.* **2012**, *30*, 1185−1194.

(2) Silverman, A. D.; Karim, A. S.; Jewett, M. C. Cell-free gene expression: an expanded repertoire of applications. *Nat. Rev. Genet.* **2020**, *21*, 151−170.

(3) Karig, D. K.; Iyer, S.; Simpson, M. L.; Doktycz, M. J. Expression optimization and synthetic gene networks in cell-free systems. *Nucleic Acids Res.* **2012**, *40*, 3763−3774.

(4) Shin, J.; Noireaux, V. Efficient cell-free expression with the endogenous *E. coli* RNA polymerase and sigma factor 70. *J. Biol. Eng.* **2010**, *4*, No. 8.

(5) Halleran, A. D.; Murray, R. M. Cell-free and in vivo characterization of Lux, Las, and Rpa quorum activation systems in *E. coli*. *ACS Synth. Biol.* **2018**, *7*, 752−755.

(6) Jayaraman, P.; Yeoh, J. W.; Jayaraman, S.; Teh, A. Y.; Zhang, J.; Poh, C. L. Cell-free optogenetic gene expression system. *ACS Synth. Biol.* **2018**, *7*, 986−994.

(7) Swank, Z.; Laohakunakorn, N.; Maerkl, S. J. Cell-free gene-regulatory network engineering with synthetic transcription factors. *Proc. Natl. Acad. Sci. U.S.A.* **2019**, *116*, 5892−5901.

(8) Senoussi, A.; Lee Tin Wah, J.; Shimizu, Y.; Robert, J.; Jaramillo, A.; Findeiss, S.; Axmann, I. M.; Estevez-Torres, A. Quantitative characterization of translational riboregulators using an in vitro transcription-translation System. *ACS Synth. Biol.* **2018**, *7*, 1269−1278.

(9) Espah Borujeni, A.; Mishler, D. M.; Wang, J.; Huso, W.; Salis, H. M. Automated physics-based design of synthetic riboswitches from diverse RNA aptamers. *Nucleic Acids Res.* **2016**, *44*, 1−13.

(10) Siegal-Gaskins, D.; Tuza, Z. A.; Kim, J.; Noireaux, V.; Murray, R. M. Gene circuit performance characterization and resource usage in a cell-free "breadboard". *ACS Synth. Biol.* **2014**, *3*, 416−425.

(11) Noireaux, V.; Bar-Ziv, R.; Libchaber, A. Principles of cell-free genetic circuit assembly. *Proc. Natl. Acad. Sci. U.S.A.* **2003**, *100*, 12672−12677.

(12) Garamella, J.; Marshall, R.; Rustad, M.; Noireaux, V. The all *E. coli* TX-TL toolbox 2.0: a platform for cell-free synthetic biology. *ACS Synth. Biol.* **2016**, *5*, 344−355.

(13) Shin, J.; Noireaux, V. An *E. coli* cell-free expression toolbox: application to synthetic gene circuits and artificial cells. *ACS Synth. Biol.* **2012**, *1*, 29−41.

(14) Takahashi, M. K.; Chappell, J.; Hayes, C. A.; Sun, Z. Z.; Kim, J.; Singhal, V.; Spring, K. J.; Al-Khabouri, S.; Fall, C. P.; Noireaux, V.; Murray, R. M.; Lucks, J. B. Rapidly characterizing the fast dynamics of RNA genetic circuitry with cell-free transcription-translation (TX-TL) systems. *ACS Synth. Biol.* **2015**, *4*, 503−515.

(15) Hu, C. Y.; Takahashi, M. K.; Zhang, Y.; Lucks, J. B. Engineering a functional small RNA negative autoregulation network with model-guided design. *ACS Synth. Biol.* **2018**, *7*, 1507−1518.

(16) Westbrook, A.; Tang, X.; Marshall, R.; Maxwell, C. S.; Chappell, J.; Agrawal, D. K.; Dunlop, M. J.; Noireaux, V.; Beisel, C. L.; Lucks, J.; Franco, E. Distinct timescales of RNA regulators enable the construction of a genetic pulse generator. *Biotechnol. Bioeng.* **2019**, *116*, 1139−1151.

(17) Hori, Y.; Kantak, C.; Murray, R. M.; Abate, A. R. Cell-free extract based optimization of biomolecular circuits with droplet microfluidics. *Lab Chip* **2017**, *17*, 3037−3042.

(18) Niederholtmeyer, H.; Sun, Z. Z.; Hori, Y.; Yeung, E.; Verpoorte, A.; Murray, R. M.; Maerkl, S. J. Rapid cell-free forward engineering of novel genetic ring oscillators. *eLife* **2015**, *4*, No. e09771.

(19) Narumi, R.; Masuda, K.; Tomonaga, T.; Adachi, J.; Ueda, H. R.; Shimizu, Y. Cell-free synthesis of stable isotope-labeled internal standards for targeted quantitative proteomics. *Synth. Syst. Biotechnol.* **2018**, *3*, 97−104.

(20) Oza, J. P.; Aerni, H. R.; Pirman, N. L.; Barber, K. W.; Ter Haar, C. M.; Rogulina, S.; Amrofell, M. B.; Isaacs, F. J.; Rinehart, J.; Jewett, M. C. Robust production of recombinant phosphoproteins using cell-free protein synthesis. *Nat. Commun.* **2015**, *6*, No. 8168.

(21) Kightlinger, W.; Lin, L.; Rosztoczy, M.; Li, W.; DeLisa, M. P.; Mrksich, M.; Jewett, M. C. Design of glycosylation sites by rapid synthesis and analysis of glycosyltransferases. *Nat. Chem. Biol.* **2018**, *14*, 627−635.

(22) Kightlinger, W.; Duncker, K. E.; Ramesh, A.; Thames, A. H.; Natarajan, A.; Stark, J. C.; Yang, A.; Lin, L.; Mrksich, M.; DeLisa, M. P.; Jewett, M. C. A cell-free biosynthesis platform for modular construction of protein glycosylation pathways. *Nat. Commun.* **2019**, *10*, No. 5404.

(23) Karim, A. S.; Jewett, M. C. A cell-free framework for rapid biosynthetic pathway prototyping and enzyme discovery. *Metab. Eng.* **2016**, *36*, 116−126.

(24) Karim, A. S.; Heggestad, J. T.; Crowe, S. A.; Jewett, M. C. Controlling cell-free metabolism through physiochemical perturbations. *Metab. Eng.* **2018**, *45*, 86−94.

(25) Dudley, Q. M.; Anderson, K. C.; Jewett, M. C. Cell-free mixing of *Escherichia coli* crude extracts to prototype and rationally engineer high-titer mevalonate synthesis. *ACS Synth. Biol.* **2016**, *5*, 1578−1588.

(26) Casini, A.; Chang, F. Y.; Eluere, R.; King, A. M.; Young, E. M.; Dudley, Q. M.; Karim, A.; Pratt, K.; Bristol, C.; Forget, A.; Ghodasara, A.; Warden-Rothman, R.; Gan, R.; Cristofaro, A.; Borujeni, A. E.; Ryu, M. H.; Li, J.; Kwon, Y. C.; Wang, H.; Tatsis, E.; Rodriguez-Lopez, C.; O'Connor, S.; Medema, M. H.; Fischbach, M. A.; Jewett, M. C.; Voigt, C.; Gordon, D. B. A pressure test to make 10 molecules in 90 days: external evaluation of methods to engineer biology. *J. Am. Chem. Soc.* **2018**, *140*, 4302−4316.

(27) Pardee, K.; Green, A. A.; Takahashi, M. K.; Braff, D.; Lambert, G.; Lee, J. W.; Ferrante, T.; Ma, D.; Donghia, N.; Fan, M.; Daringer, N. M.; Bosch, I.; Dudley, D. M.; O'Connor, D. H.; Gehrke, L.; Collins, J. J. Rapid, low-cost detection of Zika virus using programmable biomolecular components. *Cell* **2016**, *165*, 1255−1266.

(28) Takahashi, M. K.; Tan, X.; Dy, A. J.; Braff, D.; Akana, R. T.; Furuta, Y.; Donghia, N.; Ananthakrishnan, A.; Collins, J. J. A low-cost paper-based synthetic biology platform for analyzing gut microbiota and host biomarkers. *Nat. Commun.* **2018**, *9*, No. 3347.

(29) Ma, D.; Shen, L.; Wu, K.; Diehnelt, C. W.; Green, A. A. Low-cost detection of norovirus using paper-based cell-free systems and synbody-based viral enrichment. *Synth. Biol.* **2018**, *3*, No. ysy018.

(30) Salehi, A. S. M.; Yang, S. O.; Earl, C. C.; Shakalli Tang, M. J.; Porter Hunt, J.; Smith, M. T.; Wood, D. W.; Bundy, B. C. Biosensing estrogenic endocrine disruptors in human blood and urine: a RAPID cell-free protein synthesis approach. *Toxicol. Appl. Pharmacol.* **2018**, *345*, 19−25.

(31) McNerney, M. P.; Zhang, Y.; Steppe, P.; Silverman, A. D.; Jewett, M. C.; Styczynski, M. P. Point-of-care biomarker quantification enabled by sample-specific calibration. *Sci. Adv.* **2019**, *5*, No. eaax4473.

(32) Thavarajah, W.; Silverman, A. D.; Verosloff, M. S.; Kelley-Loughnane, N.; Jewett, M. C.; Lucks, J. B. Point-of-use detection of environmental fluoride via a cell-free riboswitch-based biosensor. *ACS Synth. Biol.* **2020**, *9*, 10−18.

(33) Liu, X.; Silverman, A. D.; Alam, K. K.; Iverson, E.; Lucks, J. B.; Jewett, M. C.; Raman, S. Design of a transcriptional biosensor for the portable, on-demand detection of cyanuric acid. *ACS Synth. Biol.* **2020**, *9*, 84−94.

(34) Silverman, A. D.; Akova, U.; Alam, K. K.; Jewett, M. C.; Lucks, J. B. Design and optimization of a cell-free atrazine biosensor. *ACS Synth. Biol.* **2020**, *9*, 671−677.

(35) Jung, J. K.; Alam, K. K.; Verosloff, M. S.; Capdevila, D. A.; Desmau, M.; Clauer, P. R.; Lee, J. W.; Nguyen, P. Q.; Pastén, P. A.; Matiasek, S. J.; Gaillard, J.-F.; Giedroc, D. P.; Collins, J. J.; Lucks, J. B. Cell-free biosensors for rapid detection of water contaminants. *Nat. Biotechnol.* **2020**, *38*, 1451−1459.

(36) Gräwe, A.; Dreyer, A.; Vornholt, T.; Barteczko, U.; Buchholz, L.; Drews, G.; Ho, U. L.; Jackowski, M. E.; Kracht, M.; Lüders, J.; Bleckwehl, T.; Rositzka, L.; Ruwe, M.; Wittchen, M.; Lutter, P.; Müller, K.; Kalinowski, J. A paper-based, cell-free biosensor system for the detection of heavy metals and date rape drugs. *PLoS One* **2019**, *14*, No. e0210940.

(37) Byun, J.-Y.; Lee, K.-H.; Shin, Y.-B.; Kim, D.-M. Cascading amplification of immunoassay signal by cell-free expression of firefly luciferase from detection antibody-conjugated dna in an *Escherichia coli* extract. *ACS Sens.* **2019**, *4*, 93−99.

(38) Wen, K. Y.; Cameron, L.; Chappell, J.; Jensen, K.; Bell, D. J.; Kelwick, R.; Kopniczky, M.; Davies, J. C.; Filloux, A.; Freemont, P. S. A cell-free biosensor for detecting quorum sensing molecules in *P. aeruginosa*-infected respiratory samples. *ACS Synth. Biol.* **2017**, *6*, 2293−2301.

(39) Ohashi, H.; Miyamoto-Sato, E. Towards personalized medicine mediated by in vitro virus-based interactome approaches. *Int. J. Mol. Sci.* **2014**, *15*, 6717−6724.

(40) Copeland, C. E.; Langlois, A.; Kim, J.; Kwon, Y.-C. The cell-free system: A new apparatus for affordable, sensitive, and portable healthcare. *Biochem. Eng. J.* **2021**, *175*, No. 108124.

(41) Liu, Y.; Zhan, L.; Qin, Z.; Sackrison, J.; Bischof, J. C. Ultrasensitive and highly specific lateral flow assays for point-of-care diagnosis. *ACS Nano* **2021**, *15*, 3593−3611.

(42) Wang, B.; Barahona, M.; Buck, M. Engineering modular and tunable genetic amplifiers for scaling transcriptional signals in cascaded gene networks. *Nucleic Acids Res.* **2014**, *42*, 9484−9492.

(43) Nistala, G. J.; Wu, K.; Rao, C. V.; Bhalerao, K. D. A modular positive feedback-based gene amplifier. *J. Biol. Eng.* **2010**, *4*, No. 4.

(44) Garamella, J.; Majumder, S.; Liu, A. P.; Noireaux, V. An adaptive synthetic cell based on mechanosensing, biosensing, and inducible gene circuits. *ACS Synth. Biol.* **2019**, *8*, 1913−1920.

(45) Wan, X.; Volpetti, F.; Petrova, E.; French, C.; Maerkl, S. J.; Wang, B. Cascaded amplifying circuits enable ultrasensitive cellular sensors for toxic metals. *Nat. Chem. Biol.* **2019**, *15*, 540−548.

(46) Morabito, K.; Wiske, C.; Tripathi, A. Engineering insights for multiplexed real-time nucleic acid sequence-based amplification

(NASBA): implications for design of point-of-care diagnostics. *Mol. Diagn. Ther.* **2013**, *17*, 185−192.

(47) Shaner, N. C.; Lambert, G. G.; Chammas, A.; Ni, Y.; Cranfill, P. J.; Baird, M. A.; Sell, B. R.; Allen, J. R.; Day, R. N.; Israelsson, M.; Davidson, M. W.; Wang, J. A bright monomeric green fluorescent protein derived from *Branchiostoma lanceolatum*. *Nat. Methods* **2013**, *10*, 407−409.

(48) Hostettler, L.; Grundy, L.; Kaser-Pebernard, S.; Wicky, C.; Schafer, W. R.; Glauser, D. A. The bright fluorescent protein mNeonGreen facilitates protein expression analysis in vivo. *G3: Genes, Genomes, Genet.* **2017**, *7*, 607−615.

(49) Pédelacq, J.-D.; Cabantous, S.; Tran, T.; Terwilliger, T. C.; Waldo, G. S. Engineering and characterization of a superfolder green fluorescent protein. *Nat. Biotechnol.* **2006**, *24*, 79−88.

(50) Chizzolini, F.; Forlin, M.; Yeh Martín, N.; Berloffa, G.; Cecchi, D.; Mansy, S. S. Cell-free translation is more variable than transcription. *ACS Synth. Biol.* **2017**, *6*, 638−647.

(51) Salis, H. M.; Mirsky, E. A.; Voigt, C. A. Automated design of synthetic ribosome binding sites to control protein expression. *Nat. Biotechnol.* **2009**, *27*, 946−950.

(52) Espah Borujeni, A.; Cetnar, D.; Farasat, I.; Smith, A.; Lundgren, N.; Salis, H. M. Precise quantification of translation inhibition by mRNA structures that overlap with the ribosomal footprint in N-terminal coding sequences. *Nucleic Acids Res.* **2017**, *45*, 5437−5448.

(53) Jung, S. W.; Yeom, J.; Park, J. S.; Yoo, S. M. Recent advances in tuning the expression and regulation of genes for constructing microbial cell factories. *Biotechnol. Adv.* **2021**, *50*, No. 107767.

(54) Kwok, R. Five hard truths for synthetic biology. *Nature* **2010**, *463*, 288−290.

(55) Olins, P. O.; Devine, C. S.; Rangwala, S. H.; Kavka, K. S. The T7 phage gene 10 leader RNA, a ribosome-binding site that dramatically enhances the expression of foreign genes in *Escherichia coli*. *Gene* **1988**, *73*, 227−235.

(56) de Smit, M. H.; van Duin, J. Translational standby sites: how ribosomes may deal with the rapid folding kinetics of mRNA. *J. Mol. Biol.* **2003**, *331*, 737−743.

(57) Espah Borujeni, A.; Channarasappa, A. S.; Salis, H. M. Translation rate is controlled by coupled trade-offs between site accessibility, selective RNA unfolding and sliding at upstream standby sites. *Nucleic Acids Res.* **2014**, *42*, 2646−2659.

(58) Knight, R. D.; Freeland, S. J.; Landweber, L. F. A simple model based on mutation and selection explains trends in codon and amino-acid usage and GC composition within and across genomes. *Genome Biol.* **2001**, *2*, No. research0010.

(59) Quax, T. E. F.; Claassens, N. J.; Söll, D.; van der Oost, J. Codon bias as a means to fine-tune gene expression. *Mol. Cell* **2015**, *59*, 149−161.

(60) Shu, P.; Dai, H.; Gao, W.; Goldman, E. Inhibition of translation by consecutive rare leucine codons in *E. coli*: absence of effect of varying mRNA stability. *Gene Expression* **2006**, *13*, 97−106.

(61) Lipinszki, Z.; Vernyik, V.; Farago, N.; Sari, T.; Puskas, L. G.; Blattner, F. R.; Posfai, G.; Gyorfy, Z. Enhancing the translational capacity of *E. coli* by resolving the codon bias. *ACS Synth. Biol.* **2018**, *7*, 2656−2664.

(62) Kim, J.; Copeland, C. E.; Seki, K.; Vögeli, B.; Kwon, Y.-C. Tuning the cell-free protein synthesis system for biomanufacturing of monomeric human filaggrin. *Front. Bioeng. Biotechnol.* **2020**, *8*, No. 590341.

(63) Sun, Z. Z.; Yeung, E.; Hayes, C. A.; Noireaux, V.; Murray, R. M. Linear DNA for rapid prototyping of synthetic biological circuits in an *Escherichia coli* based TX-TL cell-free system. *ACS Synth. Biol.* **2014**, *3*, 387−397.

(64) Tomanee, P.; Hsu, J. T. Transition between supercoiled and open circular plasmid DNA during alcohol precipitation. *J. Liq. Chromatogr. Relat. Technol.* **2004**, *27*, 1483−1490.

(65) Jewett, M. C.; Swartz, J. R. Mimicking the *Escherichia coli* cytoplasmic environment activates long-lived and efficient cell-free protein synthesis. *Biotechnol. Bioeng.* **2004**, *86*, 19−26.

(66) Lopreside, A.; Wan, X.; Michelini, E.; Roda, A.; Wang, B. Comprehensive profiling of diverse genetic reporters with application to whole-cell and cell-free biosensors. *Anal. Chem.* **2019**, *91*, 15284−15292.

(67) Earl, C. C.; Smith, M. T.; Lease, R. A.; Bundy, B. C. Polyvinylsulfonic acid: a low-cost RNase inhibitor for enhanced rna preservation and cell-free protein translation. *Bioengineered* **2018**, *9*, 90−97.

(68) Hunt, J. P.; Barnett, R. J.; Robinson, H.; Soltani, M.; Nelson, J. A. D.; Bundy, B. C. Rapid sensing of clinically relevant glutamine concentrations in human serum with metabolically engineered *E. coli*-based cell-free protein synthesis. *J. Biotechnol.* **2021**, *325*, 389−394.

(69) Dopp, B. J. L.; Tamiev, D. D.; Reuel, N. F. Cell-free supplement mixtures: Elucidating the history and biochemical utility of additives used to support in vitro protein synthesis in *E. coli* extract. *Biotechnol. Adv.* **2019**, *37*, 246−258.

(70) Craggs, T. D. Green fluorescent protein: structure, folding and chromophore maturation. *Chem. Soc. Rev.* **2009**, *38*, 2865−2875.

(71) Kim, J.; Copeland, C. E.; Padumane, S. R.; Kwon, Y.-C. A crude extract preparation and optimization from a genomically engineered *Escherichia coli* for the cell-free protein synthesis system: Practical laboratory guideline. *Methods Protoc.* **2019**, *2*, No. 68.

(72) Kwon, Y.-C.; Jewett, M. C. High-throughput preparation methods of crude extract for robust cell-free protein synthesis. *Sci. Rep.* **2015**, *5*, No. 8663.